Mathematical Foundations of Computing

doi:10.3934/mfc.2023042

AUTISM SPECTRUM DISORDER (ASD) CLASSIFICATION WITH THREE TYPES OF CORRELATIONS BASED ON ABIDE I DATA

Donglin Wang[✉*1], Xin Yang[✉2] and Wandi Ding[✉1]

[1]Department of Mathematical Sciences, Computational and Data Science Program, Middle Tennessee State University, United States

[2]Department of Computer Sciences, Computational and Data Science Program, Middle Tennessee State University, United States

(Communicated by Yunlong Feng)

Abstract. Autism spectrum disorder (ASD) is a type of mental health disorder, and its prevalence worldwide is estimated at about one in 100 children. Accurate diagnosis of ASD as early as possible is very important for the treatment of patients in clinical applications. ABIDE I dataset as a repository of ASD is used much for developing classifiers for ASD from typical controls. In this paper, we mainly consider three types of correlations including Pearson correlation, partial correlation, and tangent correlation together based on different numbers of regions of interest (ROIs) from only one atlas, and then twelve deep neural network models are used to train 884 subjects with 5,10,15,20-fold cross-validation on two types of split methods including stratified and non-stratified methods. We first consider six metrics to compare the model performance among the split methods. The six metrics are F1-Score, precision, recall, accuracy, and specificity, area under the precision-recall curve (PRAUC), and area under the Receiver Characteristic Operator curve (ROCAUC). The study achieved the highest accuracy rate of 71.94% for 5-fold cross-validation, 72.64% for 10-fold cross-validation, 72.96% for 15-fold cross-validation, and 73.43% for 20-fold cross-validation.

1. **Introduction.** Autism spectrum disorder (ASD) is a mental disorder, that mainly affects social communication and interaction in children. The prevalence in worldwide is estimated at about one in 100 children [43]. ASD could occur at a very young age and last throughout the patient's life. It negatively affects patients both mentally and physically. Early correct diagnosis is especially important for the treatment of patients. One common approach to diagnosing ASD is based on the Diagnostic and Statistical Manual of Mental Disorders (DSM) [4], published by the American Psychiatric Association, to observe a child's behavior and development. The correct decision needs a full evaluation of the patient according to the clinician's experience, which is more and less subjective. Resting-state functional magnetic resonance imaging (rs-fMRI), as a type of neuroimaging, has been becoming a popular approach to measuring and mapping brain activity since its

2020 *Mathematics Subject Classification.* Primary: 58F15, 58F17; Secondary: 53C35.

Key words and phrases. Autism spectrum disorder (ASD), deep learning, correlations, Regions of interest (ROIs), cross-validation.

*Corresponding author: Donglin Wang.

development, it observes the changes in oxygenation concentration Blood Oxygenation Level Dependent (BOLD) in blood flow to detect the area of activity in the brain. It has led to many remarkable studies in the medical field to understand brain functions and detect the abnormal part of the brain for disease, for example, in [18, 24, 39, 8] the authors studied the depression with fMRI, in [36, 30, 23] the authors studied attention deficit hyperactivity disorder with fMRI, in [3, 12, 38] the authors studied the Alzheimer's disease with fMRI, and there is a lot of literature on these mental disorders.

The Autism Brain Imaging Data Exchange (ABIDE) repository, as a publicly available large-scale data-sharing center of autism spectrum disorder, has been used by many researchers on different tasks since its release in 2012. There are two publicly available datasets of autism spectrum disorder (ASD) from the Autism Brain Imaging Data Exchange, namely ABIDE I and II, which is provided by https://fcon_1000.projects.nitrc.org/indi/abide/, the 1000 Functional Connectomes Project. ABIDE is a collection of structural and resting state functional MRI images from 16 international imaging sites. Classifying ASD from typical controls is one main research field based on ABIDE, and there is much literature to address the classification with different algorithms and techniques. The study [16] used two stacked autoencoders to extract lower-dimensional features as input for Support Vector Machine (SVM), Random Forest model, and a forward deep neural network (FDNN); based on 10-fold cross-validation, the FDNN gave a 70% accuracy rate. In the paper [25] the authors used a leave-one-out classifier and achieved a 60% accuracy rate, 62% sensitivity, and 58% specificity for 964 subjects. In the study [17] the authors split 816 subjects into five groups based on age, and used SVM to classify each group with 10-fold cross-validation, it achieved an accuracy, sensitivity, and specificity of 95%, 97%, and 95%, respectively for the group age larger than 30. The authors in the study [26] used six personal characteristics from 851 subjects to test nine machine learning models, based on the 10-fold cross-validation the neural network model achieved the highest accuracy rate 62.0% and area under the receiver operating characteristic curve 64.6%, sensitivity 57.1% from SVM model, specificity 72.1% from K-Nearest neighbor (KNN) model. The study [33] used a deep neural network, based on four different atlases Craddock 200 (CC200) [10] and Automated Anatomical Labelling (AAL) [34], Bootstrap Analysis of Stable Clusters (BASC) [5], and Power [27], to achieve a mean accuracy rate of 88%, sensitivity, F1-score, and area under the receiver operating characteristic curve (AUC) score of is 90%, 87%, and 96%, respectively. In the paper [14] the authors proposed a multi-input deep neural network with three atlantes, CC200, AAL, DOS160 [13] to classify 1,038 subjects, the authors used 10-fold cross-validation, 5-fold stratified cross-validation, and leave-one-site-out methods. The study achieved a classification accuracy of 78.07% on real data and 79.13% on augmented data based on an augmented set of 10,038 images. Recently, the study [40] reviewed eight different atlases to identify the most promising atlas, and the Kernel Support Vector Machine (KSVM), linear SVM, logistic regression, and deep neural model were used to achieve the highest accuracy rate of 69.43%, sensitivity 64.57%, and specificity 73.61%, based on 871 subjects with 5-fold cross-validation. The study [29] developed a novel method, called Behavior Action Recognition (BAR), to analyze untrimmed behavioral videos for diagnosing and assessing children with ASD, achieving a high accuracy rate of 79.7% for ASD from 400 ASD children and 125 with other developmental delays (ODD). The paper [1] introduced an efficient machine learning-based assessment

system, which achieves higher AUC and specificity at 90% sensitivity with a sample size of 375. The study [28] employed three deep learning models on 300 videos of ASD children in social interactions. The activity comprehension model achieved 72.32% accuracy, joint attention recognition reached up to 97%, and facial expression recognition achieved 95.1% accuracy. This study [20] evaluated the influence of technology on ASD detection, considering technological evolution, utilization of diverse bio-behavioral data, demographic factors, database management, assessment instruments, and data processing. In most of the studies, the deep learning model seems to achieve a better performance, although all the studies used different numbers of subjects.

In the realm of deep learning, empirical studies have seen notable success, but theoretical underpinnings have been lacking. Recent research is now starting to bridge this gap, providing a solid theoretical basis for practical applications. For instance, the study [15] delves into the analysis of binary classification using deep Convolutional Neural Networks (CNNs), particularly in the context of spherical datasets. They highlight the importance of understanding the discontinuity or high smoothness of objective functions, especially in relation to convex loss functions like hinge loss. The study [22] underscores the empirical accomplishments of Deep Convolutional Neural Networks (DCNNs) in various domains. However, a deeper theoretical grasp of the adaptability and feature extraction abilities of DCNNs across diverse learning tasks is still somewhat lacking. The authors introduce a versatile DCNN structure controlled by just three structural parameters, simplifying model selection. Additionally, they demonstrate DCNNs' ability to overcome dimensionality challenges in dealing with specific types of target functions. These studies bolster the theoretical framework supporting the practical application of deep learning. They fill a crucial gap between empirical success and theoretical understanding in the field.

In this paper, we proposed twelve deep neural network models with three types of correlations between nodes as input based on 884 subjects. The main contributions of this paper are: 1) most previous studies focus on only one type of correlation between nodes of the brain, we consider all three types of correlations at the same time in the models; 2) we used 5, 10, 15, and 20-fold cross-validation on two types of split methods: stratified and non-stratified methods, and the result shows a stable performance; 3) six metrics, such as F1-Score, precision, recall, accuracy, and specificity, the area under the precision-recall curve (PRAUC), and the area under the Receiver Characteristic Operator curve (ROCAUC) are used to compare the performance of models; 4) most studies used more than one atlas, in this paper four different numbers of regions of interest (ROIs) based on only one atlas [31] are used for classification, and the highest accuracy rate is 71.94% for 5-fold cross-validation, 72.64% for 10-fold cross-validation, 72.96% for 15-fold cross-validation, and 73.43% for 20-fold cross-validation.

The rest of this paper is organized as follows. In Section 2 the twelve deep neural model algorithms are introduced. In Section 3, the ABIDE I data is introduced and analyzed, and the different k-fold cross-validation models are compared. In Section 4 We close with conclusions and discussion.

2. **Methods.**

Correlation analysis as a common technique is often used in resting-state functional magnetic resonance imaging analysis (rs-fMRI), it calculates the correlation coefficient between two regions of interest (ROIs) to show the extent to which the two ROIs are connected. A higher value shows greater connectivity

between them. It is used to detect the functional connection and resting state networks in the human brain [6, 32, 7]. Suppose X and Y are two time series of two ROIs, $X = x_1, x_2, \cdots, x_t$, and $Y = y_1, y_2, \cdots, y_t$, and the Pearson correlation of the two time series is

$$r = \frac{\sum(x_i - \bar{X})\sum(y_i - \bar{Y})}{\sqrt{\sum(x_i - \bar{X})^2 \sum(y_i - \bar{Y})^2}},$$

often, the correlation values form a correlation matrix as input features in a classification task. There is one disadvantage of Pearson correlation, the value does not represent the direct connection between two ROIs, and the connection could be explained by another ROI $Z = z_1, z_2, \cdots, z_t$. The partial correlation can estimate the direct connection to find the causal relationship after removing the affection of ROI Z. The partial correlation of two ROIs X and Y, removing the affection of ROI Z is

$$r = \frac{r_{XY} - r_{XZ}r_{YZ}}{\sqrt{(1 - r_{XZ}^2)(1 - r_{YZ}^2)}}.$$

The tangent correlation [35] is another type of correlation used in fMRI analysis. By the tangent space embedding, the underlying functional connectivity can be achieved at the group level, and to some extent, this can reduce the difference among the individuals. The study [11] shows the tangent space embedding correlation outperforms the standard Pearson correlations.

The deep learning model has been used widely in many fields due to its ability to handle large-scale data and discover the latent pattern better in the data. A forward deep neural model (FDNN) includes three parts, which are the input, hidden, and output layers. For binary classification problems, the output layer contains two neurons that determine the correct class labels. The input layer consists of the m neurons, which means the m input features. The hidden layer often has more than one layer. The neurons between layers are fully connected and the current layer gets the input values from the previous layer computed by an activation function. Mathematically, let $v_{l,i}$ denote the i-th neuron of the l-th layer and k_l be the number of neurons in the l-the layer. The input layer is denoted by $v_{0,i} = x_i$ and $k_0 = m$, for each $l \geq 1$ and $1 \leq i \leq k_l$,

$$v_{k,i} = \phi\left(\sum_{j=1}^{k_{l-1}} w_{l,i,j} v_{l-1,j} + b_{l,i}\right),$$

where $w_{l,i,j} \in \mathbb{R}$, $b_{l,i} \in \mathbb{R}$, and ϕ is an activation function. The most popular choices for the activation function include the tanh, sigmoid, and rectified linear activation function (ReLU). In our study, the ReLU and the tanh functions are used in hidden layers.

To train the deep neural network model for binary classification tasks, a loss function is necessary during the training. The typical choice is binary cross-entropy. In our study, the Hinge loss function is used. It is often used in the Support Vector Machine model (SVM) for maximum-margin classification due to its ability to punish misclassifications. Our data is not balanced, so the Hinge loss function can help train the model better. The Hinge loss function has the form

$$C(y) = \max(0, 1 - yf(x)),$$

where $f(x)$ is the prediction value and y is the label of observation. The optimizer algorithm in this paper is Adam [19]. Let $\boldsymbol{\theta}$ represent the vector of all weights $w_{l,i,j}$

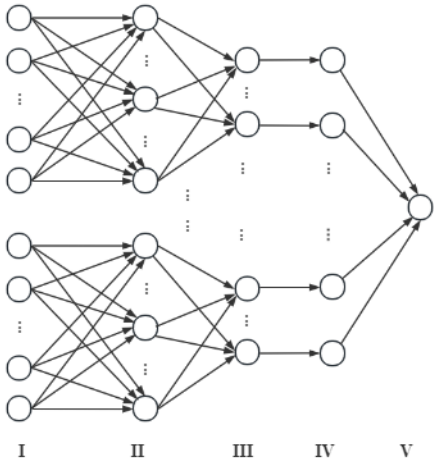

FIGURE 1. Model framework. I, II, III means hidden layer, IV means concatenated layer, and V means output.

and all bias $b_{l,i}$ parameters. The update rule at the h-th step is

$$\boldsymbol{\theta}_h = \boldsymbol{\theta}_{h-1} - \lambda \frac{\partial C}{\partial \boldsymbol{\theta}},$$

where $\lambda > 0$ is the learning rate.

In our study, a combination of twelve feedforward deep neural networks (FDNN) was trained at the same time for the classification task, and the input for each model is the different types of correlations based on the different ROIs, respectively. The framework of the combination model is illustrated in Figure 1. The combination of deep neural networks should do a better performance since it is an ensemble-like algorithm. The ensemble algorithm often shows great performance in different tasks in the machine learning field. Let's define $f(x)$ as a prediction function based on a neural network, y is the true labels with value $\{-1, 1\}$, and M neural networks are trained together, each model has the same weight of $1/M$ for the combination model. The Hinge loss function is used and has the form below.

$$\mathcal{L}(y, f(x)) = \max(0, 1 - yf(x)) = \begin{cases} 0 & \text{if } yf(x) > 1 \\ 1 - yf(x) & \text{if } yf(x) \leq 1 \end{cases}$$

and the second derivative function of this loss function is

$$\frac{\partial \mathcal{L}^2(y, f(x))}{\partial f^2(x)} = \begin{cases} \text{undefined} & \text{if } yf(X) = 1 \\ 0 & \text{otherwise} \end{cases}$$

The Hinge loss function is a continuous function and the second derivative function is non-negative although it is not differentiable at points $yf(X) = 1$, the Hinge loss function is a convex function. According to Jensen's inequality, if a function $f(x)$ is convex, there exists $f(E(x)) \leq E[f(x)]$. The Hinge loss function is a convex

function and it should apply to the inequality. There should exist

$$\mathcal{L}(y, \frac{1}{M}\sum_{i=1}^{M} f_i(x)) \leq \frac{1}{M}\sum_{i=1}^{M} \mathcal{L}(y, f_i(x))$$

$$E[\mathcal{L}(y, \frac{1}{M}\sum_{i=1}^{M} f_i(x))] \leq E[\frac{1}{M}\sum_{i=1}^{M} \mathcal{L}(y, f_i(x))]$$

$$E[\mathcal{L}(y, \bar{f(x)})] \leq \frac{1}{M}\sum_{i=1}^{M} E[\mathcal{L}(y, f_i(x))]$$

The expected loss function of combination models is less than or equal to the average of the expected loss functions of all individual models. That is to say, the combination model performs better than the individual model.

3. Case study.

3.1. Data description.

There are two publicly available datasets of autism spectrum disorder from the ABIDE, namely ABIDE I and II, which are provided by https://fcon_1000.projects.nitrc.org/indi/abide/, the 1000 Functional Connectomes Project. ABIDE is a collection of structural and resting state functional MRI images from 16 international imaging sites.

The ABIDE I data set originally included 539 autism spectrum disorders and 573 typical controls. The data was preprocessed with four different preprocessing strategies by five teams with different tools, including the Connectome Computation System (CCS), the Configurable Pipeline for the Analysis of Connectomes (CPAC), the Data Processing Assistant for Resting-State fMRI (DPARSF) and the NeuroImaging Analysis Kit (NIAK). In this study, the ABIDE I preprocessed dataset based on DPARSF is used [9]. Table 1 shows the steps and procedures based on the DPARSF strategy and more details can be found at http://preprocessed-connectomes-project.org/abide/Pipelines.html.

Table 1. DPARSF Preprocessing

Steps	Procedure
Drop first N volumes	4
Slice timing correction	yes
Motion realignment	yes
Intensity normalization	no
Motion	24-param
Tissue signals	mean WM and CSF signals
Motion realignment	yes
Low-frequency drifts	linear and quadratic trends
Band-Pass Filtering	0.01-0.1 Hz
Global Signal Regression	yes
Functional to Anatomical	rigid body
Anatomical to Standard (MNI152)	DARTEL

Due to the quality of images, the preprocessing dataset only has 884 individuals including 476 typical controls and 408 autism spectrum disorders. The original dataset and preprocessing dataset are summarized in Table 2.

TABLE 2. Summary of original data and preprocessing data

	Statistics					
	Male	Female	Total	Mean of age ± standard deviation	Minimum age	Maximum age
Original data	948	164	1,112	17.05 ±8.04	6.47	64
DPARSF preprocessing data	746	138	884	17.21 ±8.13	6.47	64

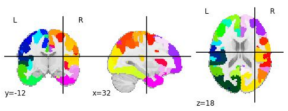

(A) 100 ROIs map

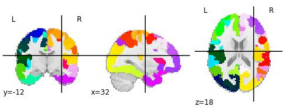

(B) 200 ROIs map

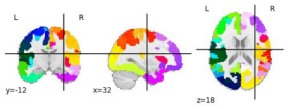

(C) 300 ROIs map

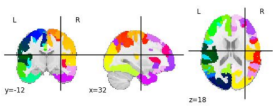

(D) 400 ROIs map

FIGURE 2. Atlas of Schaefer 2018 parcellation

3.2. **Data analysis.** The functional magnetic resonance imaging (fMRI) data is a four-dimension ($L \times W \times H \times T$) data, L is length, W is the width, H is the height, and T is the number of scans. The atlas of Schaefer 2018 parcellation [31, 41] is used to extract regions of interest (ROIs) from the preprocessing functional magnetic resonance imaging dataset. The choice of the Schaefer atlas is likely due to its suitable level of detail for the study's objectives. It strikes a balance between capturing meaningful functional subdivisions and avoiding excessive fragmentation. Additionally, previous research has successfully used the Schaefer atlas, affirming its validity and applicability for similar analyses. This study extracted 100, 200, 300, and 400 ROIs separately from each subject and the atlas maps of 100, 200, 300, and 400 ROIs used to extract signals are shown in Figure 2.

Each ROI corresponds to a time series of values with a length of T after being extracted signal. If R indicates the number of ROIs extracted, the original four-dimension data of each subject is turned into two-dimension data, $R \times T$. Three types of correlations, including Pearson correlation, partial correlation, and tangent correlation, are calculated with the package Nilearn [2] for every two ROIs of each subject, and each subject gets three symmetric matrices with dimension $R \times R$. Since there are four types of R, that means each subject has twelve symmetric matrices. Figure 3 shows the correlations for randomly chosen three subjects based on 100 ROIs.

Since all three types of matrices of correlations are symmetric, only the upper part of each matrix is used as the input feature with a dimension of $R \times (R+1)/2$, including the main diagonal values. In total, each subject has twelve features due to four different numbers of ROIs. Figure 4 shows the kernel distribution estimation of three types of correlations based on different ROIs.

A combination of twelve feedforward deep neural networks (FDNN) was trained at the same time for the classification task, and the input for each model is the different types of correlations based on the different ROIs, respectively. Each model has three hidden layers with different activation functions. The first layer has 32 neurons, the second has 32 neurons, and the third has 8 neurons. Model one, model

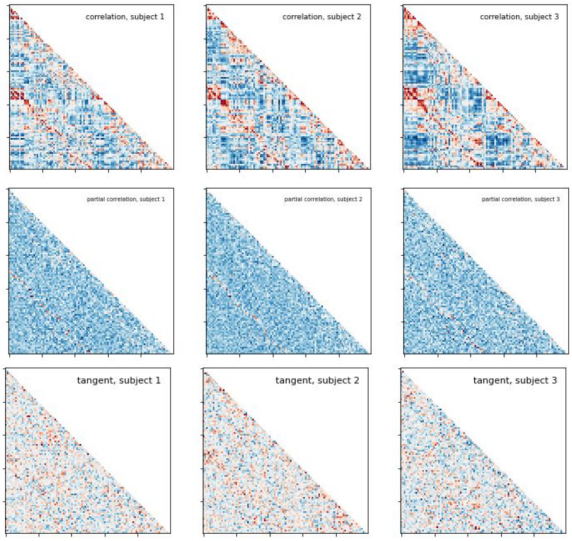

FIGURE 3. Three types of correlations based on 100 ROIs

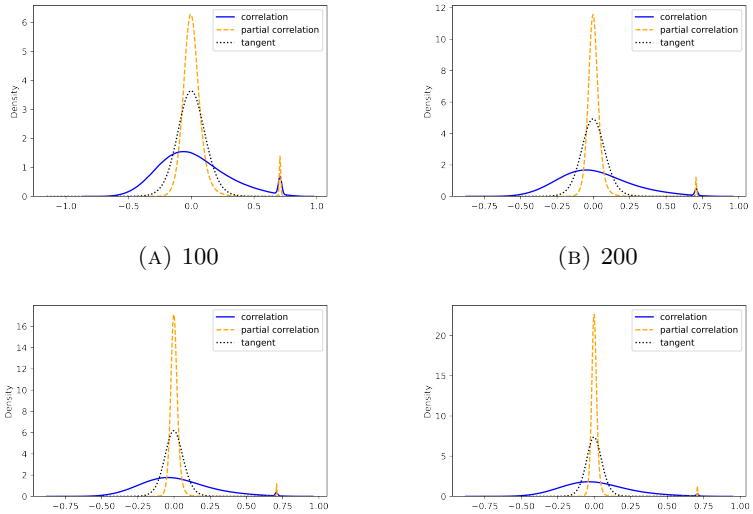

(A) 100 (B) 200

(C) 300 (D) 400

FIGURE 4. Three types of correlations between N regions for ASD and controls

two, and model three have input features from correlation, partial correlation, and tangent, respectively, based on the 100 ROIs. The features have a dimension of 5,050. The activation function for all layers is a rectified linear activation function (ReLU). Model four, model five, and model six have input features with a dimension of 20,100 based on 200 ROIs, respectively. All layers have ReLU as the activation function except the type of tangent correlation. Model seven, model eight, and

model nine have input features with a dimension of 45,150 based on 300 ROIs, respectively. All layers have tanh as the activation function. Model ten, model eleven, and model twelve have input features with a dimension of 80,200 based on 400 ROIs, respectively. All layers also have tanh as the activation function. All the outputs from the twelve models are concatenated into a dense layer. The whole model was trained with 100 epochs, and the early stopping was set to avoid overfitting by monitoring the accuracy rate of the training data with a patience number of 10. In addition, the l_2 regularization penalty was applied in the last dense output layer with a factor of 0.03. The loss function used is the Hinge function. To optimize the loss function, the Adam algorithm is used with a learning rate of 0.0001. The output is the medical status of the subject, 0 (negative case) or 1 (positive case), which means typical control or ASD. The optimal hyperparameters of the whole model are summarized in Table 3.

TABLE 3. Hyperparameters of Models

	Type	Features	Activation function	Neurons	Initializer	ROIs	Output
Model 1	correlation	5,050	ReLU, ReLU, ReLU	32, 32, 8	random normal	100	(0, 1)
Model 2	partial correlation	5,050	ReLU, ReLU, ReLU	32, 32, 8	random normal	100	
Model 3	tangent	5,050	ReLU, ReLU, ReLU	32, 32, 8	random normal	100	
Model 4	correlation	20,100	ReLU, ReLU, ReLU	32, 32, 8	random normal	200	
Model 5	partial correlation	20,100	ReLU, ReLU, ReLU	32, 32, 8	random normal	200	
Model 6	tangent	20,100	ReLU, tanh, ReLU	32, 32, 8	random normal	200	
Model 7	correlation	45,150	tanh, tanh, tanh	32, 32, 8	random normal	300	
Model 8	partial correlation	45,150	tanh, tanh, tanh	32, 32, 8	random normal	300	
Model 9	tangent	45,150	tanh, tanh, tanh	32, 32, 8	random normal	300	
Model 10	correlation	80,200	tanh, tanh, tanh	32, 32, 8	random normal	400	
Model 11	partial correlation	80,200	tanh, tanh, tanh	32, 32, 8	random normal	400	
Model 12	tangent	80,200	tanh, tanh, tanh	32, 32, 8	random normal	400	

To estimate the ability to generalize the model, the K-fold cross-validation technique is used by two types of split methods, stratified and non-stratified way. In this study, 5, 10, 15, and 20 folds are used. To estimate the performance of the models, some metrics are used. In this study, we consider seven metrics including accurate rate, precision, recall, F1-score, specificity, and the area under the receiver operating characteristic curve (ROCAUC) and the area under the precision-recall curve (PRAUC). The following formula is based on the notation in Table 4, which is the confusion matrix for binary classification.

$$precision = \frac{TP}{TP + FP} \tag{1}$$

$$recall = \frac{TP}{TP + FN} \tag{2}$$

$$F1\text{-}Score = \frac{2 * precision * recall}{precision + recall} \tag{3}$$

$$specificity = \frac{TN}{TN + FP} \tag{4}$$

$$accuracy = \frac{TP + TN}{TP + TN + FP + FN} \tag{5}$$

Precision and recall are another two common model evaluation metrics besides accuracy rate. Precision is the proportion of true positive cases (TP) among the predicted positive cases and recall is the proportion of true positive cases (TP) among the actual positive cases. F1-Score is another metric, which is the harmonic mean

TABLE 4. Confusion matrix

		True	
		ASD (Positive) $y = 1$	Controls (Negative) $y = 0$
Predict	ASD (Positive) $y = 1$	True positive (TP)	False positive (FP)
	Controls (Negative) $y = 0$	False negative (FN)	True negative (TN)

of precision and recall for a balanced purpose. Specificity is the proportion of true negative cases (TN) among the actual negative cases. The area under the receiver operating characteristic curve (ROCAUC) measures model performance across all possible classification thresholds. Basically, the higher the score, the higher the ability to predict is. Another area considered is the area under the precision-recall curve (PRAUC), which is another measure to assess model performance, especially for imbalanced datasets.

Cross-validation is a technique in machine learning to assess how well a model generalizes to new data. Stratified cross-validation ensures that different groups in the data are equally represented in both test and training sets, which is useful when we want the model to learn from all types of data. On the other hand, Non-Stratified cross-validation randomly splits the data into test and training sets without considering categories, making it suitable when we assume all categories are similar. Employing both approaches in this paper boosts our confidence in the model's ability to generalize across different scenarios. The stratified and non-stratified approaches with seven metrics based on different K-fold cross-validation models are summarized in Table 5 and in Figure 5. For the stratified approach, the 20-fold model has five metrics with higher scores except for ROCAUC compared to others. For the non-stratified approach, it seems that the 15-fold gets a slightly better performance based on precision, recall, F1-score, and accuracy rate, but the 20-fold model has a slightly higher specificity rate, ROCAUC, and PRAUC. In general, stratified and non-stratified approaches do not have a big difference based on the same k-fold method. We also summarized the performance of different models in Table 6 based on the same dataset from previous studies.

TABLE 5. Comparison of metrics for different K-fold models

Approach	K-Fold	Precision	Recall	F1-Score	Specificity	ROCAUC	PRAUC	Accuracy
Stratified	5-Fold	68.16%	68.63%	68.22%	71.98%	77.39%	74.69%	70.48%
	10-Fold	70.72%	69.82%	70.00%	74.70%	79.65%	76.51%	72.64%
	15-Fold	70.65%	70.56%	70.20%	75.48%	**79.83%**	75.59%	72.85%
	20-Fold	**70.90%**	**72.31%**	**71.23%**	**76.14%**	79.66%	**75.81%**	**73.43%**
Non-stratified	5-Fold	69.18%	70.19%	69.65%	73.34%	78.40%	74.08%	71.94%
	10-Fold	68.76%	68.11%	68.09%	73.23%	78.54%	75.46%	71.26%
	15-Fold	**70.95%**	**71.01%**	**70.38%**	74.11%	79.16%	75.35%	**72.96%**
	20-Fold	70.50%	69.73%	69.59%	**74.69%**	**80.33%**	**76.76%**	72.64%

By comparing our proposed model with previous studies, it can be seen that our model performs better under K-Fold cross-validation. Specifically, our model shows better results in terms of accuracy, recall, F1 score, specificity, ROCAUC, PRAUC, and overall accuracy in Stratified 5-Fold, 10-Fold, 15-Fold, and 20-Fold situations.

TABLE 6. Comparison of metrics for different K-fold models

Model	Observations	Type	Specificity	Sensitivity	Accuracy
DNN[16]	1,035	Pearson	63%	74%	70%
AE-MKFC [21]	1,035	Pearson	61%	-	-
DNN [42]	871	Pearson	79%	-	-
MC-NFE [37]	609	Pearson	68%	70%	63%
DNN [44]	1055	Pearson	71%	-	-

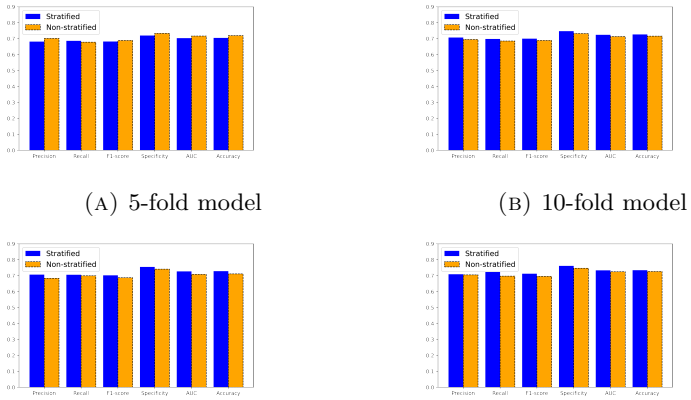

(A) 5-fold model (B) 10-fold model

(C) 15-fold model (D) 20-fold model

FIGURE 5. Plots of the mean of metrics of different K-fold models

Especially in the 20-Fold situation, our model achieves the best results in terms of accuracy, recall, and F1 score. In contrast, previous studies used different models and datasets, showing varying degrees of accuracy, specificity, and overall accuracy. Overall, our model performs better in multiple metrics, indicating higher reliability and accuracy in practical applications.

4. **Discussion and conclusion.** Three types of correlations based on four types of ROIs are used to classify ASD from typical controls in this study. A combination of twelve FDNN models is trained at the same time with the correlations from different ROIs as input. Pearson's correlation is the most common correlation to be used for detecting functional connectivity of the brain. It measures the linear relationship between two ROIs. Partial correlation is another correlation to detect the functional connectivity between two ROIs after controlling other ROIs, it measures the direct connection between any two ROIs. Tangent correlation [35] is to learn the features at the group level by the tangent space embedding. Different numbers of ROIs can cover different voxels of the brain and get as much information as possible. FDNN model is an end-to-end model that can extract features more robustly and have a better generalization ability. With different correlations from different numbers of ROIs, the combined FDNN model shows a satisfactory performance.

Four types of K-fold are used in two approaches, stratified split, and non-stratified split. For the stratified split, all six metrics are increasing slightly as k increases, except for ROCAUC. Intuitively, it makes sense since the training size is bigger and

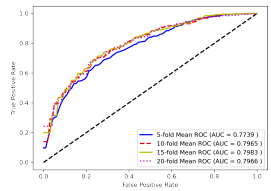

(A) Stratified ROC curve

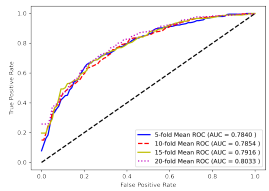

(B) Non-stratified ROC curve

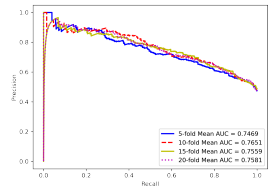

(C) Stratified PR curve

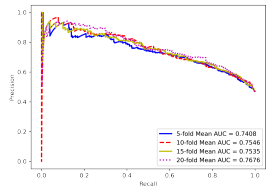

(D) Non-stratified PR curve

FIGURE 6. Plots of the mean ROC and precision-recall curves of different K-fold models

the test dataset is smaller as k is bigger. The highest scores for precision, recall, F1-score, specificity, ROCAUC, PRAUC, and accuracy are 70.90%, 72.31%, 71.23%, 76.14%, 79.83%, 76.51%, and 73.43%, respectively. For the non-stratified split, it has a similar result to the stratified approach, and the highest score for precision, recall, F1-score, specificity, ROCAUC, PRAUC, and accuracy are 70.95%, 71.01%, 70.38%, 74.69%, 80.33%, 76.76%, and 72.96%. Basically, there is just a slight difference between the two approaches based on the highest scores from the seven metrics. In order to have an intuitive comparison, we calculate the mean of different k-fold models for the two approaches. The average scores for precision, recall, F1-score, specificity, ROCAUC, PRAUC, and accuracy in the stratified approach are 70.11%, 70.33%, 69.91%, 74.58%, 79.13%, 75.65%, 72.35%, respectively, and the average scores for precision, recall, F1-score, specificity, ROCAUC, PRAUC, and accuracy are 69.85%, 69.76%, 69.43%, 73.84%, 79.11%, 75.41%, 72.20%, respectively. Based on the average score, the stratified approach has a little bit better performance. In reality, the positive case is the primary concern in the classification task, the recall score often plays an important role in ranking the model, especially for an imbalanced dataset. The dataset in this study is moderately imbalanced. Except for the recall score, F1-score and PRAUC are the other two metrics to be considered for an imbalanced dataset. For the stratified approach, the average scores of recall, F1-score, and PRAUC are 70.33%, 69.91%, and 75.65%, respectively. The average scores of recall, F1-score, and PRAUC based on the non-stratified approach are 69.76%, 69.43%, and 75.41%, respectively. The scores have no big difference for the two approaches, although the stratified approach is a little bit higher. This shows the model has a stable performance for both approaches, but in practice, the stratified approach is preferred.

Deep neural network models often provide a better performance in many applications due to their non-linear learning ability with multiple layers. The more data is used, the better the performance is. In this study, only 884 subjects are used

for the analysis, we should include the dataset of ABIDE II in the future study to improve the performance. It is reasonable to believe that the performance based on more training data will get better. In addition, there are four preprocessing pipelines including CCS, CPAC, DPARSF, and NIAK for the ABIDE I dataset. In this study, only the DPARSF preprocessing data is used in our analysis, and whether all four pipelines based on the same model provide similar performance is also the future work.

Acknowledgments. We would like to express our sincere gratitude to the reviewers for their thoughtful comments and valuable suggestions that greatly contributed to improving the quality of this paper. We also extend our thanks to the editors for their guidance and support throughout the publication process.

REFERENCES

[1] H. Abbas, F. Garberson, S. Liu-Mayo, E. Glover and D. P. Wall, Multi-modular ai approach to streamline autism diagnosis in young children, *Scientific Reports*, **10** (2020), 5014.

[2] A. Abraham, F. Pedregosa, M. Eickenberg, P. Gervais, A. Mueller, J. Kossaifi, A. Gramfort, B. Thirion and G. Varoquaux, Machine learning for neuroimaging with scikit-learn, *Frontiers in Neuroinformatics*, **8** (2014), 14.

[3] F. Agosta, M. Pievani, C. Geroldi, M. Copetti, G. B. Frisoni and M. Filippi, Resting state fmri in alzheimer's disease: Beyond the default mode network, *Neurobiology of Aging*, **33** (2012), 1564-1578.

[4] A. P. Association, *Diagnostic and Statistical Manual of Mental Disorders*, American Psychiatric Association, 5th edition, 2022. Text Revision.

[5] P. Bellec, P. Rosa-Neto, O. C. Lyttelton, H. Benali and A. C. Evans, Multi-level bootstrap analysis of stable clusters in resting-state fmri, *Neuroimage*, **51** (2010), 1126-1139.

[6] B. Biswal, F. Zerrin Yetkin, V. M. Haughton and J. S. Hyde, Functional connectivity in the motor cortex of resting human brain using echo-planar mri, *Magnetic Resonance in Medicine*, **34** (1995), 537-541.

[7] J. Cabral, M. L. Kringelbach and G. Deco, Functional connectivity dynamically evolves on multiple time-scales over a static structural connectome: Models and mechanisms, *NeuroImage*, **160** (2017), 84-96.

[8] R. L. Carhart-Harris, L. Roseman, M. Bolstridge, L. Demetriou, J. N. Pannekoek, M. B. Wall, M. Tanner, M. Kaelen, J. McGonigle, K. Murphy, et al., Psilocybin for treatment-resistant depression: Fmri-measured brain mechanisms, *Scientific Reports*, **7** (2017), 1-11.

[9] C. Craddock, Y. Benhajali, C. Chu, F. Chouinard, A. Evans, A. Jakab, B. S. Khundrakpam, J. D. Lewis, Q. Li, M. Milham, et al., The neuro bureau preprocessing initiative: Open sharing of preprocessed neuroimaging data and derivatives, *Frontiers in Neuroinformatics*, **7** (2013), 27.

[10] R. C. Craddock, G. A. James, P. E. Holtzheimer III, X. P. Hu and H. S. Mayberg, A whole brain fmri atlas generated via spatially constrained spectral clustering, *Human Brain Mapping*, **33** (2012), 1914-1928.

[11] K. Dadi, M. Rahim, A. Abraham, D. Chyzhyk, M. Milham, B. Thirion, G. Varoquaux, A. D. N. Initiative, et al., Benchmarking functional connectome-based predictive models for resting-state fmri, *NeuroImage*, **192** (2019), 115-134.

[12] E. L. Dennis and P. M. Thompson, Functional brain connectivity using fmri in aging and alzheimer's disease, *Neuropsychology Review*, **24** (2014), 49-62.

[13] N. U. Dosenbach, B. Nardos, A. L. Cohen, D. A. Fair, J. D. Power, J. A. Church, S. M. Nelson, G. S. Wig, A. C. Vogel, C. N. Lessov-Schlaggar, et al., Prediction of individual brain maturity using fmri, *Science*, **329** (2010), 1358-1361.

[14] T. M. Epalle, Y. Song, Z. Liu and H. Lu, Multi-atlas classification of autism spectrum disorder with hinge loss trained deep architectures: Abide i results, *Applied Soft Computing*, **107** (2021), 107375.

[15] H. Feng, S. Huang and D.-X. Zhou, Generalization analysis of cnns for classification on spheres, *IEEE Transactions on Neural Networks and Learning Systems*, **34** (2021), 6200-6213.

[16] A. S. Heinsfeld, A. R. Franco, R. C. Craddock, A. Buchweitz and F. Meneguzzi, Identification of autism spectrum disorder using deep learning and the abide dataset, *NeuroImage: Clinical*, **17** (2018), 16-23.
[17] A. Kazeminejad and R. C. Sotero, Topological properties of resting-state fmri functional networks improve machine learning-based autism classification, *Frontiers in Neuroscience*, **12** (2019), 1018.
[18] H. Keren, G. O'Callaghan, P. Vidal-Ribas, G. A. Buzzell, M. A. Brotman, E. Leibenluft, P. M. Pan, L. Meffert, A. Kaiser, S. Wolke, et al., Reward processing in depression: A conceptual and meta-analytic review across fmri and eeg studies, *American Journal of Psychiatry*, **175** (2018), 1111-1120.
[19] D. P. Kingma and J. L. Ba, Adam: A method for stochastic optimization, arXiv preprint, `arXiv:1412.6980`, (2014).
[20] M. Kohli, A. K. Kar and S. Sinha, The role of intelligent technologies in early detection of autism spectrum disorder (asd): A scoping review, *IEEE Access*, **10** (2022).
[21] H. Lu, S. Liu, H. Wei and J. Tu, Multi-kernel fuzzy clustering based on auto-encoder for fmri functional network, *Expert Systems with Applications*, **159** (2020), 113513.
[22] T. Mao, Z. Shi and D.-X. Zhou, Approximating functions with multi-features by deep convolutional neural networks, *Analysis and Applications*, **21** (2023), 93-125.
[23] Z. Mao, Y. Su, G. Xu, X. Wang, Y. Huang, W. Yue, L. Sun and N. Xiong, Spatio-temporal deep learning method for adhd fmri classification, *Information Sciences*, **499** (2019), 1-11.
[24] D. M. A. Mehler, M. O. Sokunbi, I. Habes, K. Barawi, L. Subramanian, M. Range, J. Evans, K. Hood, M. Lührs, P. Keedwell, et al., Targeting the affective brain-a randomized controlled trial of real-time fmri neurofeedback in patients with depression, *Neuropsychopharmacology*, **43** (2018), 2578-2585.
[25] J. A. Nielsen, B. A. Zielinski, P. T. Fletcher, A. L. Alexander, N. Lange, E. D. Bigler, J. E. Lainhart and J. S. Anderson, Multisite functional connectivity mri classification of autism: Abide results, *Frontiers in Human Neuroscience*, **7** (2013), 599.
[26] M. N. Parikh, H. Li and L. He, Enhancing diagnosis of autism with optimized machine learning models and personal characteristic data, *Frontiers in Computational Neuroscience*, **13** (2019), 9.
[27] J. D. Power, A. L. Cohen, S. M. Nelson, G. S. Wig, K. A. Barnes, J. A. Church, A. C. Vogel, T. O. Laumann, F. M. Miezin, B. L. Schlaggar, et al., Functional network organization of the human brain, *Neuron*, **72** (2011), 665-678.
[28] V. G. Prakash, M. Kohli, S. Kohli, A. P. Prathosh, T. Wadhera, D. Das, D. Panigrahi and J. V. S. Kommu, Computer vision-based assessment of autistic children: Analyzing interactions, emotions, human pose, and life skills, *IEEE Access*, **11** (2023), 47907-47929.
[29] V. G. Prakash, M. Kohli, A. P. Prathosh, M. Juneja, M. Gupta, S. Sairam, S. Sitaraman, A. S. Bangalore, J. V. S. Kommu, L. Saini, et al., Video-based real-time assessment and diagnosis of autism spectrum disorder using deep neural networks, *Expert Systems*, (2023), e13253.
[30] A. Riaz, M. Asad, E. Alonso and G. Slabaugh, Fusion of fmri and non-imaging data for adhd classification, *Computerized Medical Imaging and Graphics*, **65** (2018), 115-128.
[31] A. Schaefer, R. Kong, E. M. Gordon, T. O. Laumann, X.-N. Zuo, A. J. Holmes, S. B. Eickhoff and B. T. Yeo, Local-global parcellation of the human cerebral cortex from intrinsic functional connectivity mri, *Cerebral Cortex*, **28** (2018), 3095-3114.
[32] S. M. Smith, D. Vidaurre, C. F. Beckmann, M. F. Glasser, M. Jenkinson, K. L. Miller, T. E. Nichols, E. C. Robinson, G. Salimi-Khorshidi, M. W. Woolrich, et al., Functional connectomics from resting-state fmri, *Trends in Cognitive Sciences*, **17** (2013), 666-682.
[33] F. Z. Subah, K. Deb, P. K. Dhar and T. Koshiba, A deep learning approach to predict autism spectrum disorder using multisite resting-state fmri, *Applied Sciences*, **11** (2021), 3636.
[34] N. Tzourio-Mazoyer, B. Landeau, D. Papathanassiou, F. Crivello, O. Etard, N. Delcroix, B. Mazoyer and M. Joliot, Automated anatomical labeling of activations in spm using a macroscopic anatomical parcellation of the mni mri single-subject brain, *Neuroimage*, **15** (2002), 273-289.
[35] G. Varoquaux, F. Baronnet, A. Kleinschmidt, P. Fillard and B. Thirion, Detection of brain functional-connectivity difference in post-stroke patients using group-level covariance modeling, In *International Conference on Medical Image Computing and Computer-Assisted Intervention*, Springer, (2010), 200-208.

[36] D. Wang, D. Hong and Q. Wu, Attention deficit hyperactivity disorder classification based on deep learning, *IEEE/ACM Transactions on Computational Biology and Bioinformatics*, **20** (2023), 1581-1586.
[37] N. Wang, D. Yao, L. Ma and M. Liu, Multi-site clustering and nested feature extraction for identifying autism spectrum disorder with resting-state fmri, *Medical Image Analysis*, **75** (2022), 102279.
[38] S. L. Warren and A. A. Moustafa. Functional magnetic resonance imaging, deep learning, and alzheimer's disease: A systematic review, *Journal of Neuroimaging*, **33** (2023), 5-18.
[39] Q.-Z. Wu, D.-M. Li, W.-H. Kuang, T.-J. Zhang, S. Lui, X.-Q. Huang, R. C. K. Chan, G. J. Kemp and Q.-Y. Gong, Abnormal regional spontaneous neural activity in treatment-refractory depression revealed by resting-state fmri, *Human Brain Mapping*, **32** (2011), 1290-1299.
[40] X. Yang, N. Zhang and P. Schrader, A study of brain networks for autism spectrum disorder classification using resting-state functional connectivity, *Machine Learning with Applications*, **8** (2022), 100290.
[41] B. T. Yeo, F. M. Krienen, J. Sepulcre, M. R. Sabuncu, D. Lashkari, M. Hollinshead, J. L. Roffman, J. W. Smoller, L. Zöllei, J. R. Polimeni, et al., The organization of the human cerebral cortex estimated by intrinsic functional connectivity, *Journal of Neurophysiology*, (2011).
[42] W. Yin, S. Mostafa and F.-X. Wu, Diagnosis of autism spectrum disorder based on functional brain networks with deep learning, *Journal of Computational Biology*, **28** (2021), 146-165.
[43] J. Zeidan, E. Fombonne, J. Scorah, A. Ibrahim, M. S. Durkin, S. Saxena, A. Yusuf, A. Shih and M. Elsabbagh, Global prevalence of autism: A systematic review update, *Autism Research*, **15** (2022), 778-790.
[44] J. Zhang, F. Feng, T. Han, X. Gong and F. Duan, Detection of autism spectrum disorder using fmri functional connectivity with feature selection and deep learning, *Cognitive Computation*, **15** (2023), 1106-1117.

Received May 2023; 1st revision September 2023; 2nd revision October 2023; early access October 2023.